ARTICLE OPEN

Check for updates

Classification and spatial mapping of atmospheric corrosion of China

Wenkui Hao[1], Lingling Xu[2], Xin Chen[1]✉, Yan Jin[3], Yu Han[1]✉, Xinghui Zhang[3], Yun Chen[1], Luyao Huang[1], Bingkun Yang[1], Zhixiang Zhu[1] and Xiaofang Wang[1]

Atmospheric corrosion is ubiquitous in China but varies a lot among different regions covering the cold, temperate, and tropical zones. Categorizing the atmospheric corrosivity and plotting precise atmospheric corrosion map remain key interest for a variety of industries. The present work proposed an atmospheric corrosion map of China for hot-dip galvanized steels, which was constructed by inverse distance weighting (IDW) interpolation algorithm based on both the measured corrosion rates of coupons exposed at 2393 inland test stations and calculated corrosion rates from a prevalent dose-response function in 2918 sites in coastal regions. When the corrosion category was used as the criterion, the IDW interpolation algorithm of power 2 performed best. Cross-validation results confirmed that the prediction accuracy of IDW interpolation reached 85.6%. Based on the corrosion map, the categories of atmospheric corrosivity in China could be determined.

npj Materials Degradation (2022)6:100 ; https://doi.org/10.1038/s41529-022-00315-4

INTRODUCTION

Atmospheric corrosion refers to a spontaneous degradation process of metals resulting from interactions with its surrounding environmental variables (e.g. relative humidity (RH) and temperature) and accumulative atmospheric contaminants (e.g. deposition of chlorides and sulfides), which is the most common type of corrosion that widely influences multiple industries such as infrastructure, transportation and manufacturing[1–3]. Atmospheric corrosion is estimated to account for more than half of all corrosion damages[4,5]. Quantifying the accurate area of different corrosion categories is an important step in raising awareness of the seriousness of corrosion issues, particularly relevant to decision makers in the industry and government—such that better policies can be established to improve our ability for mitigating corrosion risks in severe corrosion area. Differentiated materials selection and efficient corrosion protection based on corrosivity classification become a key to sustain integrity of the metallic facilities and equipment and reduce corrosion costs for different industries[6].

A precise atmospheric corrosion map provides an important guide to differentiated materials selection and economical engineering design since it enables a visual cue for the identification of atmospheric corrosion category and prediction of service life of metals and coatings in any given region. Plotted in the 1960s, the atmosphere corrosion map of the British Isles has been known as the pioneer trying to visualize the effect of atmospheric corrosion[7]. Subsequently, the atmospheric corrosion maps of different countries and cities, including Switzerland, Brazil, Spain, Korea, Slovakia, Thailand, Vietnam, Abu Dhabi, and Istanbul have been drawn for the assessment of their atmospheric corrosion risks[8–16]. Plotting precise atmospheric corrosion map has been of great interest to corrosion scientists and engineers in China for many decades. Since the 1990s, China has conducted a number of differently scaled studies on the corrosion map in certain areas exposed to diverse corrosion environments[17]. Based on the corrosion data of carbon steel exposed in 20 corrosion sites, Wang et al.[18] drew the atmospheric corrosion map of Hainan province. Fan et al.[19] constructed an atmospheric corrosion map of Shandong province by using 1-year corrosion rate of hot-dip galvanized steel from 100 exposure corrosion test sites. Huang et al.[20] collected a set of corrosion data of Q235 steel from 48 sites and drew an atmospheric corrosion map of Guangdong province, China. However, a nationwide atmospheric corrosion map lacked for a long time in consideration of vast territory and diverse climates in China.

The biggest challenge in corrosion map optimization is how to improve the accuracy of the map so that to provide local corrosion data with high precision. The accuracy of the map is firstly supported by plenty of corrosion data derived from sufficient on-site atmospheric exposure sites. On the basis of one-year on-site exposure tests at 21 sites both in marine and urban regions, Kim et al.[21] constructed an atmospheric corrosion map of Korea. Vera et al.[22] collected the corrosion data of carbon steel and galvanized steel after one-year exposure in 31 stations in Chile and developed a national map of corrosion. Kumar et al.[23] constructed an atmospheric corrosion map of India by collecting corrosion data in 32 stations consecutively. However, considering the vast territory and climate changes in these countries, such a scale of corrosion sites is not able to meet the demand of drawing a corrosion map with high resolution. Also, on-site exposure corrosion tests are usually established in urban area to reduce the manpower and the cost of corrosion data collection. Less exposure sites were set up in rural area and natural environments, where large infrastructure construction, like power lines and high speed railway, suffer from serious corrosion and deterioration. The accurate corrosion categories in these regions face challenges. To better predict the atmospheric corrosion in these regions, different statistical or parametric models regarding corrosion prediction in correlation with environmental factors were proposed based on long-term atmospheric environmental metal corrosion tests[24,25]. They include dose-response functions (DRFs), developed for several common metals based on regression analysis that have been used

[1]State Key Laboratory of Advanced Power Transmission Technology, State Grid Smart Grid Research Institute Co.,Ltd., 102209 Beijing, China. [2]HVDC Technical Center of State Grid Corporation of China, 100052 Beijing, China. [3]State Grid Corporation of China, 100032 Beijing, China. ✉email: chenxin1@geiri.sgcc.com.cn; hanyugeiri@163.com

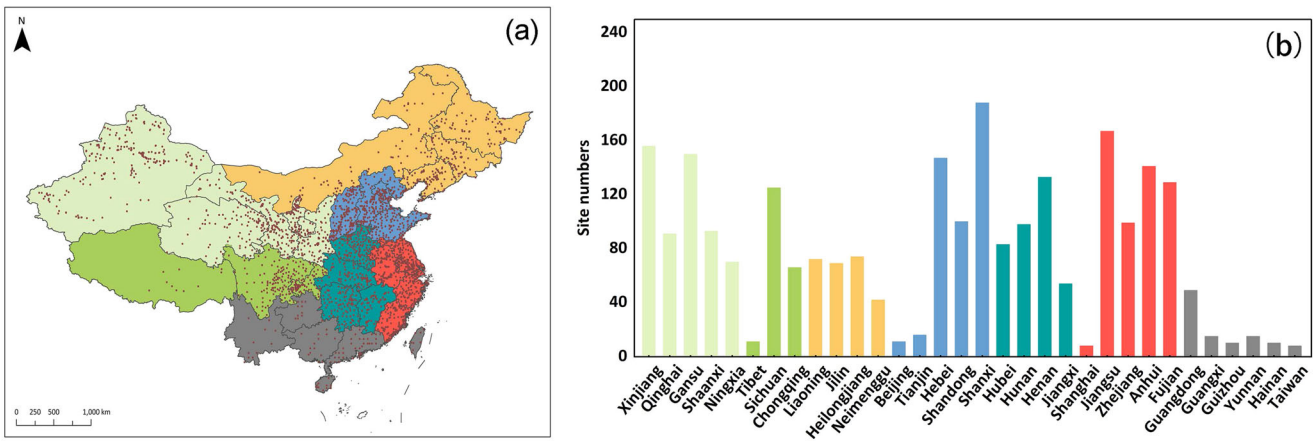

Fig. 1 The distribution of the corrosion stations in China. a The distribution of outdoor corrosion stations; **b** the amount of outdoor corrosion stations in different provinces.

for the prediction of atmospheric corrosion rate of metals[26–28]. DFRs are currently more popular since they are simpler and do not require large-scale outdoor exposure tests to obtain corrosion data[29]. ISO 9223 recommends a DRF to predict the first-year corrosion rate of four typical metals, including carbon steel, zine, copper, and aluminum, based on temperature, RH, annual average Cl^- deposition, and annual average SO_2 deposition[30]. Based on this, some researchers introduced more environmental parameters into the power function and proposed more sophisticated DRFs regarding corrosion prediction. The UN/ECE ICP Materials project proposed a set of DRFs described with RH, temperature, sulfur dioxide, nitrogen dioxide, ozone, rainfall, rainfall acidity, and particulate matter, which is suitable for mapping and calculations of cost of corrosion damage[31]. However, the prediction accuracy of DRFs in different climates varies largely. Castañeda et al.[25] prososed that the DRFs of ISO 9223 may over estimate corrosion rate in tropical region and under estimate corrosion rate in Asia region. The prediction accuracy of the corrosion map may be reduced sharply when large corrosion data from DRFs are used in interpolation calculation.

In the mapping process, interpolation techniques such as inverse distance weighting (IDW) interpolation algorithm have been applied in atmosphere corrosion. IDW is a deterministic method, which assumes that the value of the point decreases in weight or influence as it increases in distance from that point[32]. The power parameter within the IDW tool controls the weight of individual points, which can be used to increase the accuracy of the interpolation method. However, the validity of the interpolation algorithm were not discussed[33,34]. This study attempted to draw a precise atmospheric corrosion map of China to provide guidance to corrosion mitigation of industrial engineering. One year on-site exposure tests was firstly carried out using hot-dip galvanized steel at 2393 stations in China. Chloride distribution equation was also proposed to better predict corrosion rate along coastal area by using the DRFs presented in ISO 9223. Based on this, an optimized atmospheric corrosion map of the study area was drawn by IDW interpolation algorithm. After running the interpolations, a cross validation was performed on each of the predicted surfaces. This work provides a nationwide category of atmospheric corrosivity, which will strongly support the differentiated materials selection and efficient corrosion protection in China.

RESULTS AND DISCUSSION

Category of corrosivity of atmosphere in China

ISO 9223 standard recommends a classification of the corrosivity of the atmospheric environments by dividing the one-year corrosion rate data of typical metal materials obtained from on-site atmospheric exposure sites into six categories, from low to high, are C1, C2, C3, C4, C5, and CX, respectively. In this study, the corrosion of galvanized steel sample in the first year can be considered as the corrosion of zinc. The distribution of the test stations are presented in Fig. 1 and the corresponding corrosion categories of galvanized steel is shown in Fig. 2. More than 85% of the corrosion exposure stations (i.e., 2034 stations) are located in mild corrosion zones, among which C2 accounts for 44.24% of the total, C3 is 41.11% and C1 is only 2.64%. C4, C5, and CX represent relatively high corrosion rates. About one-tenth of the corrosion exposure stations lies on C4 area and 1.79% in C5 area. Notably, about 1% of the corrosion exposure stations are located in CX region, which are considered as extreme corrosion risk.

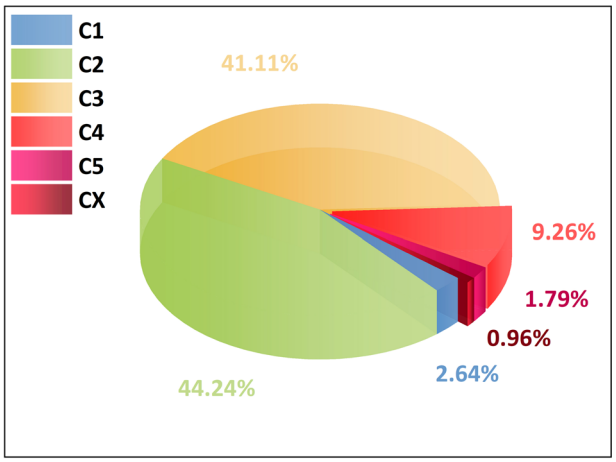

Fig. 2 Results of corrosion categories of galvanized steel according to ISO 9223. The atmospheric environments are dividing into six categories, from low to high, are C1, C2, C3, C4, C5, and CX, respectively.

More specifically, the corrosion categories of galvanized steel in different provinces of China are shown in Fig. 3. According to geographical and climatic differences, these provinces are divided into six parts, Northwest China, Southwest China, Northeast China, North China, Central China, Eastern China, and South China. The corrosion category distribution of the exposure stations appears some regularity in spite of its variation in various province. The proportion of exposure stations in heavily corroded area (C4 and above) gradually increased from the northwest to the southeast of

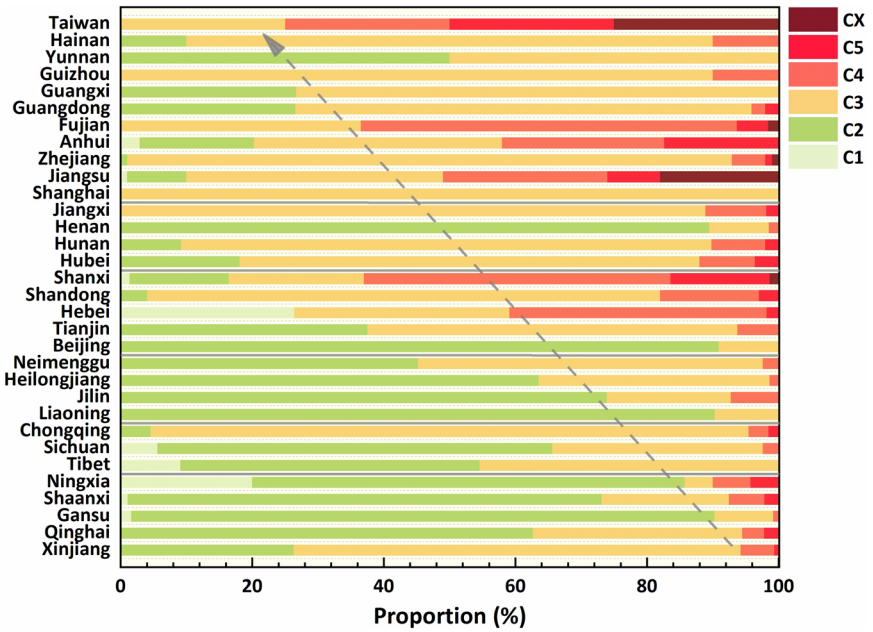

Fig. 3 Results of corrosion categories of galvanized steel in different provinces according to ISO 9223. The corrosivity of the atmospheric environments in different provinces.

China. Except for Xinjiang province, most stations are located in C2 area in the five provinces Northwest, suggesting a relatively mild corrosion risk. C3 category occupied almost 70% of the stations in Xinjiang province, which may be attributed to the huge difference in geographical conditions. Most of the stations are located in humid climate regions, where human activities and industrial production occurs (Fig. 1b). In Southwest China, more than 90% of stations are located in C3 category in Chongqing municipality, while more slight corrosion categories were observed in Tibet and Sichuan province. High relative humidity and abundant rainfall account for the increased corrosion risk in Chongqing municipality. As for Tibet, more stations are needed to enrich the essential corrosion data and determine more precise corrosion categories. In North China, notably, a significant increase of station numbers of C4 categories was observed in Shanxi and Hebei provinces compared the other 3 provinces, which is because of the large number of coal mines that lead to a higher concentration of pollutants in the atmosphere in this area. The most severe corrosion risk was observed in Eastern China and South China, especially in coastal regions in Zhejiang, Fujian, Guangdong, Guangxi, Hainan, and Taiwan, where more than 50% of stations located in C4-CX categories, suggesting that a comprehensive corrosion protection is urgently needed to the application, operation and maintenance of metal materials.

Chloride ion diffusion model in coastal region

Chloride is one of the most detrimental factors to corrosion, especially in the coastal regions. It is quite well-known that chloride over the continent decays exponentially as a function of increasing distance from the coastline[35]. The classification of atmospheric corrosion may change rapidly with the increasing distance from the coastline in consideration of the rapid decrease of Cl^- deposition rate with the distance from the coastline. Table 1 shows the deposition rate of chloride for different environment monitor stations along the distance to the coastline. Though the 3 stations were located at different latitudes in coastal regions, the annual average Cl^- deposition showed a similar decline tendency. The annual average Cl^- deposition were plotted as a function of distance to the sea as shown in Fig. 4a. Cl^- deposition rate is the highest at the shore and sharply decreases within 1 km from the shoreline (Fig. 4b). At the distance >1 km, the decay is gradually decreasing. Significantly, the increase of Cl^- deposition rate at 8 km can be attributed to the fact that the diffusion of chloride ions was blocked by buildings, trees, and shelters[13]. Based on these data, a chloride ion diffusion model in the coastal region is proposed as followed:

$$y = 43.23x^{-0.47}, R^2 = 0.91 \quad (1)$$

wherein x and y are the distance to the sea and chloride ion deposition rate, respectively. A similar chloride distribution pattern was observed in the model proposed by cole et al.[36,37] An exceptionally high Cl^- deposition rate occurred at the shoreline and dropped suddenly as the distance from the sea increased within the first km. Compared with the model in the coastal region of Guangdong province proposed by Chen et al.[38], based on only 4 exposure sites were proposed 200 m away from the shoreline, the chloride diffusion model in our work are more reasonable to satisfy the "fast followed by slow" trend. Based on this model, 2918 sites in coastal provinces were selected to calculate their chloride ion deposition rates according to the above equation.

Dose-response function in coastal region

Metals are exposed to hundreds of times more chloride in the coastal region than that inland, which lead to severe corrosion of metals and further major insecurity of infrastructures. Due to the limitation of the field tests, the corrosion exposure data are insufficient in the coastal region, especially for test sites within 0–1 km from the coastline, which leads to inaccuracy of corrosion category estimation. To solve this problem, a DRF recommended by ISO 9223, incorporating annual average Cl^- deposition, annual average SO_2 deposition, temperature and RH, was used to evaluate the corrosivity in 2918 sites within 0-30 km from the coastline. Annual average Cl^- deposition in different sites were calculated by the chloride ion diffusion model proposed in this study. While annual average SO_2 deposition, temperature and RH were designated by the annual average values proposed in Table 2. Compared with the Cl^- deposition, the temperature, RH and SO_2 deposition rate remained relatively stable in coastal regions. Combined with the measured corrosion data in 2393 inland stations, the calculated corrosion data participate in the

Table 1. The deposition rate of chloride for environment monitor stations along the distance to the coastline.

Stations		1	2	3	4	5	6	7	8
Distance to the coastline (km)		0.01	0.1	1.7	4	7	8	15	30
Annual Cl^- deposition ($mg{\cdot}m^{-2}{\cdot}d^{-1}$)	Fujian province	195	98.37	58.14	21.54	33.13	31.16	14.65	8.22
	Liaoning province	182.2	/	/	27.94	/	18.21	13.09	6.3
	Shandong province	178.9	108	54.6	/	33.9	/	12.13	8.16
Annual average Cl^- deposition ($mg{\cdot}m^{-2}{\cdot}d^{-1}$)		185.4	103.2	56.4	24.7	33.5	24.7	13.29	7.56

interpolation to improve the accuracy of the corrosion map. The equation for zinc is expressed as:

$$r_{corr} = 0.0129P_d^{0.44}\exp(0.046\mathrm{RH} + f_{Zn}) + 0.0175S_d^{0.57}\exp(0.008\mathrm{RH} + 0.085T) \quad (2)$$

$$f_{Zn} = 0.038(T-10)T \le 10^{\circ}\mathrm{C}\; f_{Zn} = -0.071(T-10)T > 10^{\circ}\mathrm{C}$$

where r_{corr} is first-year corrosion rate of zinc (μ ma^{-1}); P_d and S_d are the annual average SO_2 deposition and annual average Cl^- deposition (mg m^{-2} d^{-1}), respectively; T and RH represent the annual average temperature (°C) and relative humidity (%), respectively; f_{Zn} is a correlation coefficient of Zn. Combining the average temperature, RH provided by local meteorological department and observed sulfur dioxide deposition rate in coastal stations, the corrosion rates of zinc in 2918 coastal points were calculated, together with the observed corrosion rates inland, to serve as interpolation data.

Atmospheric corrosion map of China

Based on the first-year corrosion rate (μ ma^{-1}) of galvanized steel obtained from 2393 exposure test sites and calculated corrosion rates from a prevalent DRF in 2918 sites in coastal regions, the atmospheric corrosion map of China was constructed by using the IDW spatial interpolation method.

Figure 5 shows the atmospheric corrosion maps obtained by IDW spatial interpolation method with powers of 1, 2, 3, and 4. The search radius was flexible with nearest 10 points participating in interpolation calculation. The distribution of corrosivity categories is consistent with different powers, that is, the corrosivity of the atmosphere in the coastal region is significantly higher than that in the inland region, which is consistent with the actual observed data.

After running the interpolations, a cross validation was performed on 700 points selected from different provinces. It compares measured values with the predicted ones from the predicted surface. The mean relative error (MRE), mean absolute error (MAE), and root-mean-square error (RMSE) of interpolation results are shown in Table 3. With the increase of power values, the MRE, MAE, and RMSE decreased at first and then increased, suggesting that IDW interpolation algorithm of power 2 performed best in the prediction of corrosion rate. The average MRE was the smallest with a value of 25.74% when the power was 2, which is reasonable on the basis that the study area covers more than 9.6 million square kilometers. The average MAE and RMSE of the interpolation results in the presence of power 2 were 0.2414 and 0.3018, respectively. All the three cross validation methods suggested that the power parameter of IDW interpolation algorithm is reasonable to ensure the accuracy of the interpolation method.

In main industrial sectors, like infrastructure, energy, transportation, and manufacturing, corrosion scientists and engineers focus principally on the atmospheric corrosion category rather than the accurate corrosion rate in the project location. Thus, counting the accuracy of atmospheric corrosion category through cross validation should be considered a more important reference. The predicted corrosion rates in the extracted points were compared with measured corrosion rates in those stations and the result is shown in Table 4. Based on the prediction results, the atmospheric corrosion categories of 575 sites are consistent with the observed results, suggesting a prediction accuracy of 82.1% in the presence of power 1. The atmospheric corrosion categories of 93 stations are 1 grade different (higher or lower) compared with the corrosion categories calculated from those stations. Only 26 stations showed a 2 grade difference of the corrosion categories, which was mainly impacted by long distance and local contamination in the surrounding sites. The IDW of power 2 performed best. The predicted atmospheric corrosion categories of 599 sites are consistent with observed results. Only 10.7% and 3.7% of sites showed a difference of 1 and 2 corrosion categories, respectively. As for the power 3 and 4, there are 83% and 80.4% of the calculated sites presented the same atmospheric corrosion category compared with the observed stations.

The corresponding area and proportion of different corrosion categories with power 2 are listed in Table 5. The vast majority of the studied area, with proportions of 50.07% and 44.14%, lies in C2 and C3 areas staining with green and yellow, respectively. C2 occurs more in Southwest China and Northeast China, whereas C3 is more likely to appear in Northwest China and Eastern China. In addition, it was estimated that the C1 category (very low) mainly exists in Xizang, western Sichuan, and Ningxia provinces, accounting for only 1.72% of the study area. C4-CX categories account for only 4.07% (390,760 km^2) of the study area, which displays cluster distribution in south and southeast coastal provinces including Zhejiang, Fujian Guangdong, Guangxi, Hainan, Taiwan, and patchy distribution in inland provinces like Shanxi, Hebei, and Hubei. Notably, though only 0.34% and 0.12% is dedicated to C5 and CX areas, respectively, a mass of metallic facilities and equipment served in infrastructure, transportation, manufacturing, and public services face a dramatically increased corrosion risk on the basis that C5 and CX areas are precisely where the most economically developed regions in China.

In summary, a precise atmospheric corrosion map of China was plotted by using IDW interpolation algorithm in this study. Both the measured corrosion rates of hot-dip galvanized steel coupons exposed in 2393 test stations inland and calculated corrosion rates from a prevalent DRF in 2918 sites in coastal regions were employed to construct the map. The precision of IDW interpolation algorithm was evaluated by cross validation. The important findings include:

1. A chloride ion diffusion model in coastal region is proposed. Chloride deposition rate decreases exponentially with increasing distance from the sea.

2. The atmospheric corrosion map shows C2 (50.07%) and C3 (44.14%) zones cover the vast majority of the study area. C4-CX categories account for 4.07% (390760 km^2) of the study area in China.

3. Cross-validation results demonstrated that the prediction accuracy of IDW interpolation algorithm was 85.6%

4. The atmospheric corrosion map of the study area can be used to improve our capacity for corrosion protection, operation maintenance, and life prediction for outdoor engineering materials in severe corrosion area.

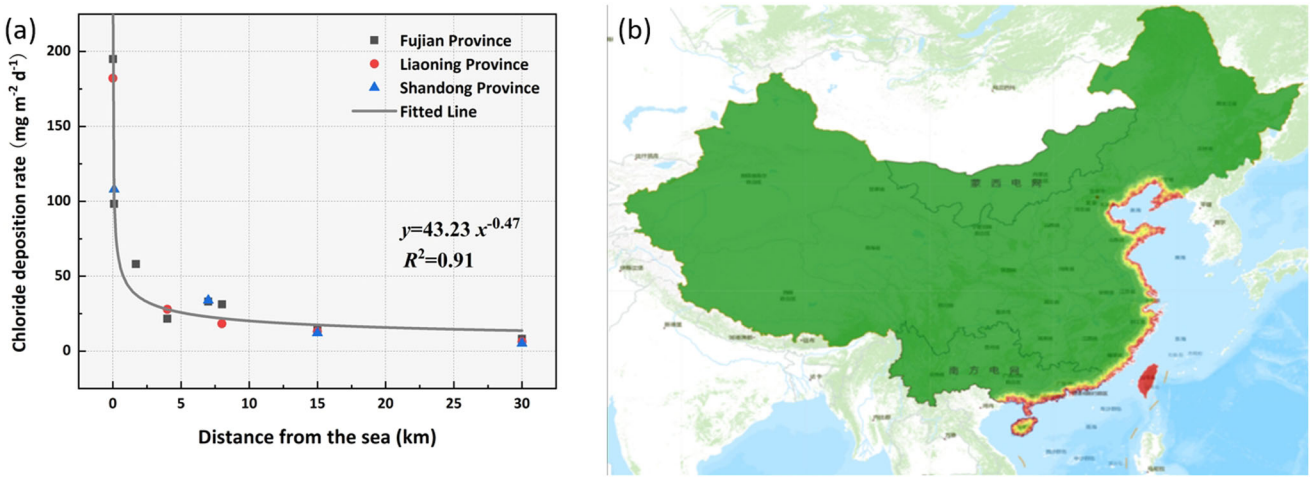

Fig. 4 The change of chloride ion distribution in coastal region. a the chloride ion diffusion model; **b** the chloride ion distribution map of coastal region in China.

Table 2. The annual average values of corrosion factors collected from monitoring stations.

Stations		Annual average temperature	Annual average relative humidity	Annual average SO_2 deposition
Unit		°C	%	$mg{\cdot}m^{-2}{\cdot}d^{-1}$
Liaoning Province	1	11.8	59.9	16.8
	2	11.2	61.7	17.4
	3	10.8	60.3	20.5
	4	10.6	54.9	19
Hebei Province	5	14.5	58.2	24.6
	6	14.2	56.4	20.1
	7	14.2	58	23.2
Tianjin City	8	15.9	54.6	16.9
Shandong Province	9	15.4	65.9	20.9
	10	14.6	60.2	27
Jiangsu Province	11	16.2	71	15.9
	12	16.4	69.3	17
	13	15.9	72.9	17.9
	14	16	67.5	16.2
Shanghai City	15	17.4	73.5	11.7
Zhejiang Province	16	17.6	75.6	12
	17	18.4	76.2	9.6
	18	18.3	77.5	8.9
	19	18.9	76.9	11
	20	18.2	77.3	10.7
	21	18	76.8	10.5
Fujian Province	22	19.8	75	10.2
	23	20.4	76.3	10.6
	24	20.6	74.8	9.4
	25	21.2	77.1	8.8

METHODS

Exposed materials and methods

Hot-dip galvanized steel coupons with dimensions of $150 \times 70 \times 3\ mm^3$ were used in this study. The initial thickness of the zinc coating was no less than 86 μm, which was consistent with the production requirements in China. Coupons were all numbered and ultrasonically rinsed with deionized water and ethanol for 15 min (for 15 min in each solution). Before the expose test, the initial weights of the cleaned coupons were recorded by an electronic balance (Me 204, Mettler Toledo, precision ± 0.1 mg). The samples were mounted on shelves with the lowest position at 1 m above the ground, facing south with a slant angle of 45°. After one-year exposure tests, all the coupons were retrieved at each test station and the corrosion products were removed guided by ISO 9226[39]. The corrosion rate (r_{corr}) of each coupon was calculated using the following equation:[40]

$$r_{\mathrm{corr}} = \frac{3.65 \times 10^3 \times (w_0 - w_t)}{s \times t \times d} \quad (3)$$

where r_{corr} is the corrosion rate, expressed in grams per square meter per year ($g\ m^{-2}\ a^{-1}$); w_0 and w_t represent the weights before and after the test, expressed in gram (g); s, t and d stand for the sample area expressed in square meter (m^2), test time expressed in year (a) and material density expressed in grams per cubic centimeter ($g\ cm^{-3}$). Triplicate samples were used for each test station to ensure the reproducibility of the results.

Atmospheric on-site exposure test

Atmospheric on-site exposure tests were conducted at 2393 corrosion test stations in China. Part of the corrosion data were collected from literatures[20]. The details and geographical position distribution of the test stations are presented in Fig. 1. Three key principles were proposed in the optimized selection of test stations, including the uniform distribution principle to ensure at least one station in every 1000~1500 km^2, a moderate increase of the number of test stations in heavy corrosion environments and emphasis on differentiated environments and climate.

Environmental parameters collection

In this study, relevant environmental parameters including temperature, *RH*, and SO_2 deposition rate were collected and the results were statistically averaged at 25 cities in costal region. The weather data were obtained from the Meteorological Department during the exposure test. SO_2 deposition was collected by PbO_2 cylinder method recommended by ISO 9225[41]. Table 2 shows the annual average values of temperature, *RH* and SO_2 deposition in different stations. Particularly, Cl^- deposition rate was measured by dry gauze method along the vertical direction of coastline in 3 coastal cities. Table 1 shows the distance from the coastline for the collection sites and the average

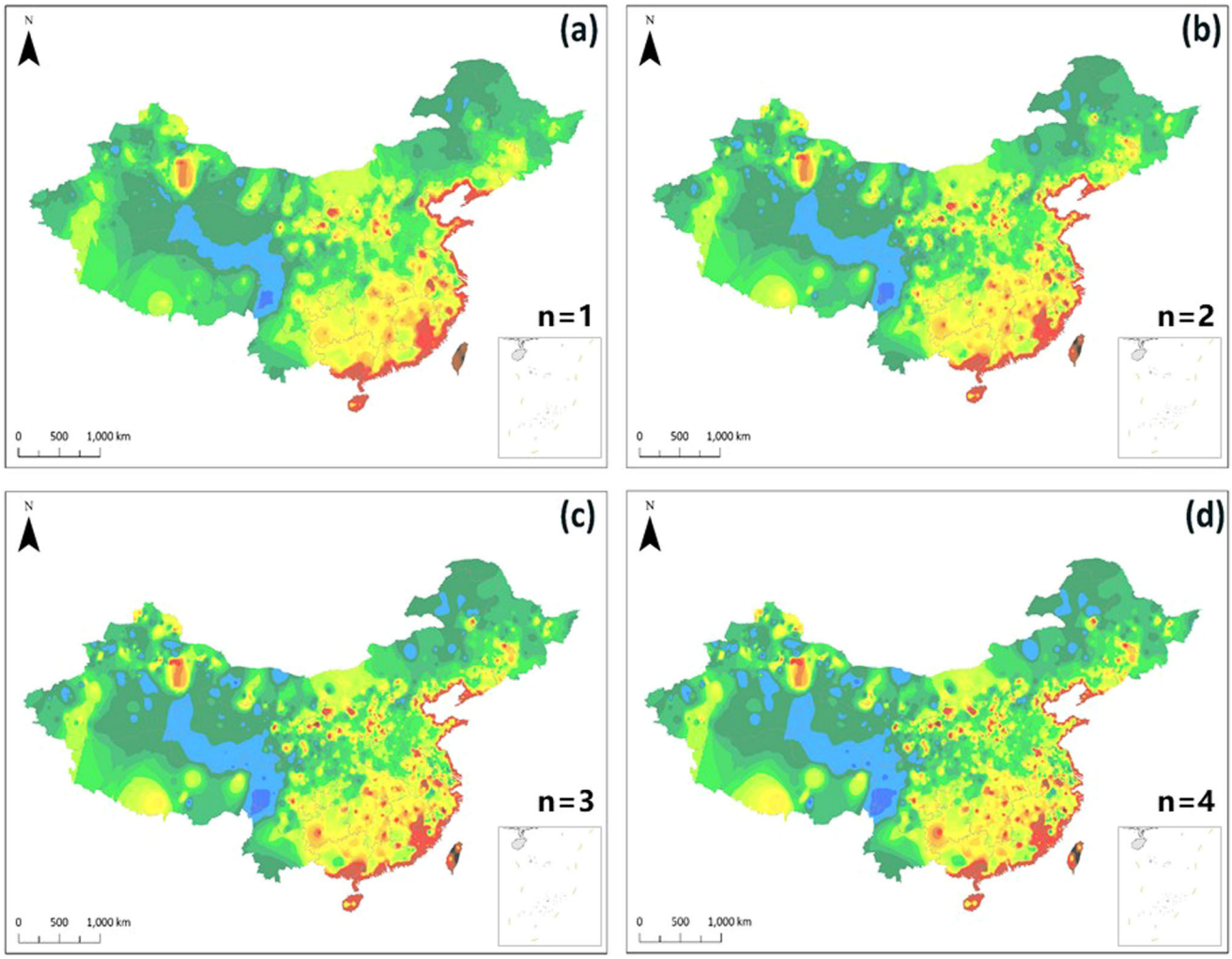

Fig. 5 The atmospheric corrosion map of China with powers of 1, 2, 3, and 4. a $n = 1$; **b** $n = 2$; **c** $n = 3$; **d** $n = 4$.

Table 3. The MRE, MAE, and RMSE of interpolation results by cross validation.

P value	Numbers of stations	MRE (%)	MAE (μm/a)	RMSE (μm/a)
1	700	27.23	0.272	0.331
2	700	25.74	0.241	0.302
3	700	28.15	0.245	0.354
4	700	30.12	0.265	0.361

Cl^- deposition rate. Double-layered dry gauze was fixed by a plastic frame with a diameter of 120 mm under the shelter of a perspex hood with the exposure orientation always facing the coastline. After monthly exposure, dry gauzes were extracted from exposure racks and analyzed to obtain the chloride ion deposition rate guided by ISO 9225. Based on the results, a modified chloride ion diffusion model in the coastal region of China was proposed. Finally, the corrosion rate was calculated via the DRF proposed by ISO 9223 from a 30-kilometer area around the coastline.

Atmospheric corrosion map

According to ISO 9223, the atmospheric corrosion can be divided into 6 categories from very low to extreme: C1, C2, C3, C4, C5, and CX. Based on the measured corrosion rate of hot-dip galvanized steel coupons exposed in 2393 test stations inland and calculated corrosion rate from DRF in 2918 sites around the coastline, in this work, the atmospheric corrosivity categories of these stations of China were determined.

To visualize the atmospheric corrosion map, the data of the collected cities were linked to their corresponding geographical coordinates and translated into colors on a map through ArcGIS software (version 10.4). Firstly, the longitudes and latitudes of the stations were put into ArcGIS software to mark out their corresponding locations on the map of China. Secondly, the corrosion rates of the stations were given to corresponding locations. Then the presented values of the whole country are computed based on IDW interpolation algorithm. To improve the accuracy of the atmospheric corrosivity map and optimize the visual experience, each category was divided into several sub-categories dyed with the similar color scheme.

IDW interpolation algorithm explicitly works on the assumption that things which are closer to each other are more alike than those which are farther apart[42]. The interpolated values are essentially estimated by the local weighted averages, as shown in formulas (3) and (4):

$$Z_0 = \sum_{i=1}^{n} Z_i \lambda_i \tag{4}$$

$$\lambda_i = \frac{\frac{1}{d^p}}{\sum_{i=1}^{n} \frac{1}{d_i^p}} \tag{5}$$

Table 4. Statistics of sites corrosion categories prediction results by cross validation.

	Power = 1		Power = 2		Power = 3		Power = 4	
	Numbers	Proportion (%)	Numbers	Proportion (%)	Numbers	Proportion (%)	Numbers	Proportion (%)
Consistent category	575	82.1	599	85.6	581	83	563	80.4
One category difference	93	13.3	75	10.7	95	13.6	101	14.4
Two categories difference	32	4.6	26	3.7	24	3.4	36	5.2

Table 5. The area and proportion of different corrosion categories.

Corrosion category	Area (km^2)	Proportion (%)
C1	165,140	1.72
C2	4,807,220	50.07
C3	4,236,880	44.14
C4	346,600	3.61
C5	32,640	0.34
CX	11,520	0.12

in which Z_0 and Z_i are the estimated value at a predicted point and the observed value at a given point, respectively; λ_i is the weight value, which is a positive real number; n represents the number of sampled points used for the estimation. Greater values of p grant greater influence on values which are closest to the point to be interpolated[43]. The parameter prediction for the target location is a summation of the product of 'allotted weights' and 'measured values' for all sites. After reviewing numerous literature, p is taken to be 1–4 for the current study to optimize the atmospheric corrosion map.

Cross Validation

Cross validation was carried out in 700 stations in China to evaluate the performance of IDW interpolation algorithm. After extracted from the interpolation, the predicted corrosion rate is estimated by the observed data obtained from the closest 10 stations[44]. Then the predicted corrosion rate is compared with the extracted data. Both the corrosion rate and corrosion category of 700 stations and the results can be statistically analyzed. Three statistical methods were employed in this study include MAE (Eq. (5)), MRE (Eq. (6)), and RMSE (Eq. (7)), respectively.

$$\mathrm{MAE} = \frac{1}{n}\sum_{i=1}^{n}|Z_i - Z_0| \tag{6}$$

$$\mathrm{MRE} = \frac{1}{n}\sum_{i=1}^{n}\frac{|Z_i - Z_0|}{Z_i} \tag{7}$$

$$\mathrm{MRSE} = \sqrt{\frac{1}{n}\sum_{i=1}^{n}(Z_i - Z_0)^2} \tag{8}$$

where Z_0 and Z_i are the predicted corrosion rate and the corresponding observed corrosion rate at point i at the same point, respectively. The smaller the values of MAE, MRE, and MRSE, the higher the interpolation precision.

DATA AVAILABILITY

The data presented in this article is available upon request to the authors.

Received: 11 October 2022; Accepted: 10 December 2022;
Published online: 27 December 2022

REFERENCES

1. Koushik, B. G., Steen, N. V., Mamme, M. H., Ingelgem, Y. V. & Terryn, H. Review on modelling of corrosion under droplet electrolyte for predicting atmospheric corrosion rate. *J. Mater. Sci. Technol.* **62**, 254–267 (2021).
2. Roberge, P. R., Klassen, R. D. & Haberecht, P. W. Atmospheric corrosivity modeling — a review. *Mater. Des.* **23**, 321–330 (2002).
3. Lebozec, N., Jönsson, M. & Thierry, D. Atmospheric corrosion of magnesium alloys: influence of temperature, relative humidity, and chloride deposition. *Corrosion* **60**, 356–361 (2004).
4. Hou, B. R. et al. The cost of corrosion in China. *npj Mater. Degrad.* **1**, 1–10 (2017).
5. Kumar, V., Sharma, N., Tiwari, S. K. & Kango, S. Atmospheric corrosion of materials and their effects on mechanical properties: a brief review. *Mater. Today* **44**, 4677–4681 (2021).
6. Zhi, Y. J., Yang, T. & Fu, D. M. An improved deep forest model for forecast the outdoor atmospheric corrosion rate of low-alloy steels. *J. Mater. Sci. Technol.* **49**, 202–210 (2020).
7. Slamova, K. & Koehl, M. Measurement and GIS-based spatial modelling of copper corrosion in different environments in Europe. *Mater. Corros.* **68**, 20–29 (2017).
8. Reiss, D., Rihm, B., Thöni, C. & Faller, M. Mapping stock at risk and release of zinc and copper in Switzerland-dose response functions for runoff rates derived from corrosion rate data. *Water Air Soil Poll.* **159**, 101–113 (2004).
9. Sica, Y. C., Kenny, E. D., Portella, K. F., & Campos Filho, D.F. Atmospheric corrosion performance of carbon steel, galvanized steel, aluminum and copper in the north Brazilian coast. *J. Braz. Chem. Soc.* **18**, 153–166 (2007).
10. Chico, B., Fuente, D., Vega, J. M. & Morcillo, M. Corrosivity maps of Spain for zinc in rural atmospheres. *Rev. Metal.* **46**, 485–492 (2010).
11. Kim, Y. S., Lim, H. K., Kim, J. J. & Park, Y. S. Corrosivity of atmospheres in the Korean peninsula. *Corros. Sci. Technol.* **10**, 109–117 (2011).
12. Ivaskova, M., Kotes, P. & Brodnan, M. Air pollution as an important factor in construction materials deterioration in Slovak Republic. *Proc. Eng.* **108**, 131–138 (2015).
13. Pongsaksawad, W., Klomjit, P., Khamsuk, P., Sorachot, S. & Pålsson, N. S. Chloride distribution model and corrosion map of structural steels for tropical climate in Thailand. *Sci. Total Environ.* **787**, 147465 (2021).
14. Ganther, W. D. et al. Towards the development of a corrosion map for Abu Dhabi. *Mater. Corros.* **62**, 1066–1073 (2011).
15. Karaca, F. Mapping the corrosion impact of air pollution on the historical peninsula of Istanbul. *J. Cult. Herit.* **14**, 129–137 (2013).
16. Cole, I., Corrigan, P. & Hue, N. V. Steel corrosion map of Vietnam. *Corros. Sci. Technol.* **11**, 103–107 (2012).
17. Wu, D. Q. et al. Prediction of polycarbonate degradation in natural atmospheric environment of China based on BP-ANN model with screened environmental factors. *Chem. Eng. J.* **399**, 125878 (2020).
18. Wang, Z. Y., Chen, H. C., Yu, G. C. & Han, W. Investigation on atmospheric corrosiveness in hainan province. *J. Iron Steel Res. Int.* **10**, 59–62 (2003).
19. Fan, Z. B., Li, X. G., Jiang, B., Wang, X. M. & Wang, Q. Mapping atmospheric corrosivity in Shandong. *Water Air Soil Pollut.* **231**, 569 (2020).
20. Huang, J. C., Meng, X. B., Zheng, Z. J. & Gao, Y. Optimization of the atmospheric corrosivity mapping of Guangdong Province. *Mater. Corros.* **70**, 91–101 (2019).
21. Kim, Y. S., Lim, H. K., Kim, J. J., Hwang, W. S. & Park, Y. S. Corrosion cost and corrosion map of Korea – based on the data from 2005 to 2010. *Corros. Sci. Technol.* **10**, 52–59 (2011).
22. Vera, R., Puentes, M., Araya, R., Rojas, P. & Carvajal, A. Atmospheric corrosion map of Chile: results after one year of exposure. *Rev. Constr.* **11**, 61–72 (2012).
23. Kumar, V. & Sil, A. Rubric assessment and spatial zonal mapping of atmospheric corrosion of steel in India. *Corrosion* **77**, 795–808 (2021).
24. Tidblad, J. et al. UN ECE ICP Materials: dose-response functions on dry and wet acid deposition effects after 8 years of exposure. *Water Air Soil Poll.* **130**, 1457–1462 (2001).

25. Castañeda, A. A., Corvo, F., Fernández, D. & Valdés, C. Outdoor-indoor atmospheric corrosion in a coastal wind farm located in a tropical island. *Eng. J.* **21**, 43–62 (2017).
26. Benarie, M. & Lipfert, F. L. A general corrosion function in terms of atmospheric pollutant concentrations and rain pH. *Atmos. Environ.* **20**, 1947–1958 (1986).
27. Panchenko, Y. M. et al. Comparative estimation of long-term predictions of corrosion losses for carbon steel and zinc using various models for the Russian territory. *Corros. Eng. Sci. Technol.* **52**, 149–157 (2017).
28. Zhi, Y. J. et al. Improving atmospheric corrosion prediction through key environmental factor identification by random forest-based model. *Corros. Sci.* **178**, 109084 (2021).
29. Mikhailov, A. A. Estimating and mapping the material corrosion losses in the European part of Russia with unified doze—response functions. *Prot. Met* **38**, 281–296 (2002).
30. ISO 9223. *Corrosion of metals and alloys — Corrosivity of atmospheres — Classification, determination and estimation* (2012).
31. Kucera, V. et al. UN/ECE ICP materials dose-response functions for the multi-pollutant situation. *Water Air Soil Poll.* **7**, 249–258 (2007).
32. Castillo-Miranda, J. O. & Rodriguez-Gomez, F. J. Mapping of the cost of atmospheric corrosion of zinc and galvanised steel due to the effect of atmospheric pollution in the Mexico City Metropolitan area. *Corros. Eng. Sci. Technol.* **57**, 408–419 (2022).
33. Omran, E. S. E. Improving the prediction accuracy of soil mapping through geostatistics. *Int J. Geosci.* **3**, 574–590 (2012).
34. Kambezidis, H. D. & Kalliampakos, G. Mapping atmospheric corrosion on modern materials in the Greater Athens area. *Water Air Soil Poll.* **224**, 1463 (2013).
35. Guan, H., Love, A. J., Simmons, C. T., Makhnin, O. & Kayaalp, A. S. Factors influencing chloride deposition in a coastal hilly area and application to chloride deposition mapping. *Hydrol. Earth Syst. Sc.* **14**, 801–813 (2010).
36. Cole, I. S., Paterson, D. A. & Ganther, W. D. Holistic model for atmospheric corrosion Part 1 –Theoretical framework for production, transportation and deposition of marine salts. *Corros. Eng. Sci. Technol.* **38**, 129–134 (2003).
37. Cole, I. S. et al. Holistic model for atmospheric corrosion Part 2 – Experimental measurement of deposition of marine salts in a number of long range studies. *Corros. Eng. Sci. Technol.* **38**, 259–266 (2003).
38. Chen, H., Cui, H. Y., He, Z. B., Lu, L. & Huang, Y. H. Influence of chloride deposition rate on rust layer protectiveness and corrosion severity of mild steel in tropical coastal atmosphere. *Mater. Chem. Phys.* **259**, 123971 (2021).
39. ISO 9226. *Corrosion Of Metals And Alloys — Corrosivity Of Atmospheres — Determination Of Corrosion Rate Of Standard Specimens For The Evaluation Of Corrosivity* (2012).
40. Hai, C. et al. Analysis of corrosion evolution in carbon steel in the subtropical atmospheric environment of sichuan. *J. Mater. Eng. Perform.* **30**, 8014–8022 (2021).
41. ISO 9225. *Corrosion Of Metals And Alloys — Corrosivity Of Atmospheres — Determination Of Corrosion Rate Of Standard Specimens For The Evaluation Of Corrosivity* (2012).
42. Lu, G. Y. & Wong, D. W. An adaptive inverse-distance weighting spatial interpolation technique. *Comput Geosci.-UK* **34**, 1044–1055 (2008).
43. Shukla, K., Kumar, P., Mann, G. S. & Khare, M. Mapping spatial distribution of particulate matter using Kriging and Inverse Distance Weighting at supersites of megacity Delhi. *Sustain Cities Soc.* **54**, 101997 (2020).
44. Denby, B. et al. Spatial mapping of ozone and SO_2 trends in Europe. *Sci. Total Environ.* **408**, 4795–4806 (2010).

ACKNOWLEDGEMENTS

This work is supported by the Science and Technology Project of the Headquarters of State Grid Corporation of China (No. 5200-202058470A-0-0-00).

AUTHOR CONTRIBUTIONS

W.K.H. designed the experiments, analyzed the results, and wrote the paper. L.L.X., X.C., Y.J., and X.H.Z. contributed to the outdoor corrosion tests. Y.C., B.K.Y., Z.X.Z., and X.F.W. were responsible for data processing. Y.H. and L.Y.H. revised the paper. All the authors contributed to the interpretation of the experimental data.

COMPETING INTERESTS

The authors declare no competing interests.

ADDITIONAL INFORMATION

Correspondence and requests for materials should be addressed to Xin Chen or Yu Han.